Structural Analysis of Carboline Derivatives As Inhibitors of MAPKAP K2 Using 3D QSAR and Docking Studies

Ravi Shashi Nayana,[†] Suneel Kumar Bommisetty,[†] Kriti Singh,[†] Santhosh Kumar Bairy,[†] Sivakumari Nunna,[‡] Akula Pramod,[†] and Ravikumar Muttineni*,[†]

Biocampus, S-1, Phase-1, Technocrats Industrial Estate, Balanagar, Hyderabad, A.P., India − 500 037, and Bioinformatics Division, Environmental Microbiology Laboratory, Department of Botany, Osmania University, Hyderabad 500 007, A.P, India − 500 037

MAPKAPK2, a substrate of p38 MAPKs, plays central role in p38-mediated signal transduction, and its inhibitors are promisingly useful in the treatment of inflammatory diseases. The computational approaches comprising both ligand-based drug design and structure-based drug design were used as virtual screening strategies for the discovery of novel MK2 inhibitors. Two quantitative pharmacophore models were generated with a training set of 27 MK2 inhibitors using HypoGen module of CATALYST. The two models suggested that two hydrogen bond acceptors, one hydrogen bond donor, and one hydrophobic feature are essential for ligand binding. Further, 3D QSAR model with comparative molecular field analysis (CoMFA) and comparative molecular similarity index analysis (CoMSIA) was constructed using a training set of 42 inhibitors. The predictive CoMFA and CoMSIA models have cross-validated coefficients (q^2) of 0.804 and 0.765 and regression coefficients (r^2) of 0.984 and 0.986, respectively. The structure-based studies were carried out by docking 77 known MAPKAPK2 inhibitors into the active site of receptor using Glide and analyzing the "hotspots" of the active site. Docking studies revealed that Met138, Leu141, Asp207, Lys93, Cys140, Leu70, Thr206, and Gly143 are showing interactions with highly active compounds. The structure activity relationships elucidated here for carboline derivatives combined with their binding information will provide an integrated approach to explore the chemical space further for improving the potency of MAPKAPK2 inhibitors.

1. INTRODUCTION

Protein kinases have become major class of druggable targets in the pharmaceutical industry and a number of low molecular mass inhibitors are in the clinic now.[1,2] The role of the stress-activated p38 MAPK/SAPK2 protein kinase cascade[3] in the inflammatory processes has been defined several years ago by the anti-inflammatory effect of the p38 MAPKα, β/SAPK2a, b inhibitor SB203580, and other related compounds.[4] The discovery of MAPK inhibitors (PubChem accession numbers: SB203580, SB239063, and RWJ67657) have been central to the investigations delineating the role of this pathway in the disease process.

Accordingly, it was expected that the several components of p38 MAPK/SAPK2 protein kinase cascade may be essentially involved in the early signaling of the inflammatory response and, hence are one of the suitable targets for an anti-inflammatory therapy. Substantially, it was observed from the homologous recombination studies in mice that the deletion of one of the two known specific upstream activators of p38 MAPK/SAPK2, such as the dual-specific MAPK kinase MKK3, leads to a reduction in IL-12 production,[5] and targeted disruption of the Mkk3 gene impaired tumor necrosis factor alpha (TNF-α) induced cytokine expression.[6]

Interestingly, mice lacking one of the several kinases downstream to p38 MAPK/SAPK2, that is, serine/threonine kinase MK2,[7] also showed a reduction in the bacterial LPS-induced biosynthesis of TNF-α, interferon-gamma (IFN)-γ, interleukin-1 (IL-1), interleukin-6 (IL-6), and nitric oxide,[8] suggesting that MK2 is a key regulator of the inflammatory processes.[9]

MK2 is a direct substrate of p38 alpha and p38 beta MAPKs,[10] and is responsible for many of the signaling events that follow the activation of these MAPKs.[11] However, in vivo experiments revealed that the MAPKAP-K2 (MK2) is activated by a distinct MAP kinase homologue termed stress-activated protein kinase-2 (SAPK-2), also known as p38,[12] p40,[13] RK,[14] CSBP,[15] and Mxi2.[16] It also regulates the inflammatory cytokines such as TNF-α, IL-6, and IFN-γ through a post-transcriptional mechanism.[17−19] Tumor necrosis factor alpha (TNF-α) has been implicated in many inflammatory diseases, such as rheumatoid arthritis (RA), inflammatory bowel disease, and psoriasis. To date, several anti-TNF-α biologics including Enbrel, Remicade, and Humira have been approved for use as anti-inflammatory therapies.[20] This evidence demonstrates the multiple roles of MK2 in the inflammatory mechanisms and strengthen the suitability of the protein to be used as a druggable target for the discovery of anti-inflammatory molecules.

MAPKAP-K2 consists of a proline-rich N-terminal domain, a catalytic domain that is most similar (35−40% identity) to the subfamily that includes Ca²⁺/calmodulin-

* To whom correspondence should be addressed. Phone: +91 9989899074. E-mail address: ravambio@gmail.com.
† Biocampus, S-1, Phase-1, Technocrats Industrial Estate.
‡ Osmania University.

dependent protein kinases, and a C-terminal tail that contains a putative nuclear localization signal.[21] In vitro results elucidated the activation mechanism of MAPKAP-K2 by SAPK-2 via phosphorylation of Thr222 and Ser272 in the catalytic domain and Thr-334 in the C-terminal tail. Phosphorylation of any two of these three residues is sufficient for maximal activation.[22] It was found that when KB cells are stimulated with sodium arsenite, these residues also become phosphorylated in an SB203508 sensitive manner.[22]

Discovery of the three-dimensional pharmacophores that can explain the activity of a series of ligands is one of the most significant contributions of computational chemistry to drug discovery.[23] Three-dimensional quantitative structure−activity relationship (3D QSAR) programs such as the HypoGen module of CATALYST, CoMFA, and CoMSIA aim at using three-dimensional alignments of molecules for quantitative prediction of the activity. 3D QSAR models are more interpretable than 2D descriptor or fingerprint-based QSAR models, making it easier to suggest new compounds for synthesis using these computational tools. It would also be possible to make relational conclusions from activity and structure-based models, either for adding more information that overlay for the construction of a pharmacophore model[24] or to use a pharmacophore to assist in the refinement of protein homology models.[25,26] Here, we report the detailed study on carboline derivatives as MK2 inhibitors, seeking insights into the structural requirements and binding affinities. The binding modes of these inhibitors were explored by performing docking studies.

2. RESULTS AND DISCUSSION

2.1. Pharmacophore Studies. A total of 77 carboline analogs having inhibitory activity against MK2 receptor were collected from the literature.[27] The three-dimensional structures were constructed by using SYBYL programming package (version 6.7). Geometric optimizations of the compounds were done using the semiempirical program MOPAC 6.0, applying the AM1 Hamiltonian, and were used as starting points for conformational analyses. These structures were imported into CATALYST for conformers and pharmacophore generation. The conformational space of each inhibitor was extensively sampled utilizing the poling algorithm employed within the CONFIRM module of CATALYST. Conformational coverage was performed employing the "Best" module to ensure the extensive sampling of the conformational space (see section 4.3 under Molecular Modeling). To decode the spatial arrangement of structural features necessary for the biological activity, quantitative 3D pharmacophore models were built using the CATALYST-HYPOGEN module. The HYPOGEN enumerates possible pharmacophoric features of the high active compounds, which may complement the receptor's binding site. It implements an optimization algorithm that evaluates a large number of potential models within the pharmacophoric space of a particular target and does not perform the evaluation if the generated conformers exceeds a count of 2.[17] The extent of the evaluated space is indicated by the configuration (Config.) cost of each modeling run and should not exceed 17 for any HYPOGEN run. We considered 27 training set compounds, on the basis of structural diversity, which covered all ranges of activity for the generation of 3D

pharmacophore models. We considered the common features (hydrogen bond acceptor, hydrogen bond donor, and hydrophobic) that are present in the high active compounds to generate the hypothesis. When the models are generated without any constraints on the selected features they were showing a configuration cost greater than 17. Restricting the pharmacophoric space might improve the efficiency of optimization by allowing effective evaluation of a limited number of pharmacophoric models. Instead of the default range of zero to five for vector features, we restricted the HYPOGEN to explore pharmacophoric models incorporating from zero to two for HBA and HBD and zero to three for hydrophobic features, respectively. Furthermore, the software was constrained to explore pharmacophores with a minimum of four features. This confinement allows generating optimum features necessary to complement the feature-rich nature of MK2 binding pocket.

Each HYPOGEN run generated 10 optimal pharmacophoric hypotheses, and each run was automatically ranked according to their corresponding "total cost" values (total cost is defined as the sum of error cost, weight cost, and configuration cost, for details see Pharmacophore Validation under Molecular Modeling). HYPOGEN also calculates the cost of the null hypothesis, which presumes that there is no relationship in the data and that experimental activities are normally distributed about their mean values. Accordingly, the greater the difference between the null hypothesis cost and total cost, the more significant is the correlation (if the cost difference is >60 the significance of the hypothesis will be greater than 90%). Two significant pharmacophore models (Figure 1) were obtained in two different runs, one containing the features hydrogen bond acceptor (A), hydrogen bond donor (D), hydrogen bond donor (D), hydrophobic (H) (HypoA) and another with hydrogen bond acceptor (A), hydrogen bond acceptor (A), hydrogen bond donor (D), hydrophobic (H) (HypoB). The total and null cost of best hypothesis of HypoA (HypoA1) was 94.584 and 244.791, respectively. The best hypothesis of HypoB (HypoB1) was having the total and null cost values of 96.070 and 225.659, respectively. Statistical details of the two hypotheses are listed in Table 1. On comparison of the statistics for the best models in the two runs, HypoB1 was found to have higher internal prediction (0.973) and lower rms (0.760) values than those of HypoA1. Although HypoB1 is marginally superior in case of internal prediction, the two pharmacophore models are more than 90% statistically significant because both are having a cost difference greater than 60. The two pharmacophore models (HypoA1 and B1), along with its intrafeature distances are shown in the Figure 1. These models are having three features in common, that is, one hydrogen bond acceptor (HBA), one hydrogen bond donor (HBD), and one hydrophobic feature (HY), and also their intrafeature distances are close. When the two pharmacophore models were mapped to the most active (**67**) compound in the training set (Figure 2), they showed identical mapping of these three features to the compound: one HBA is mapped to sulfur of thiazole ring, HBD to NH of amide group between thiazole, and piperidine ring and HY to methyl-substituted fused piperidine ring. The second hydrogen bond donor of HypoA1 was mapping to the NH of fused piperidine ring and the second HBA of HypoB1 was superimposing on to the CO of fused piperidine ring.

INHIBITORS OF MAPKAP K2

J. Chem. Inf. Model., Vol. 49, No. 1, 2009   **55**
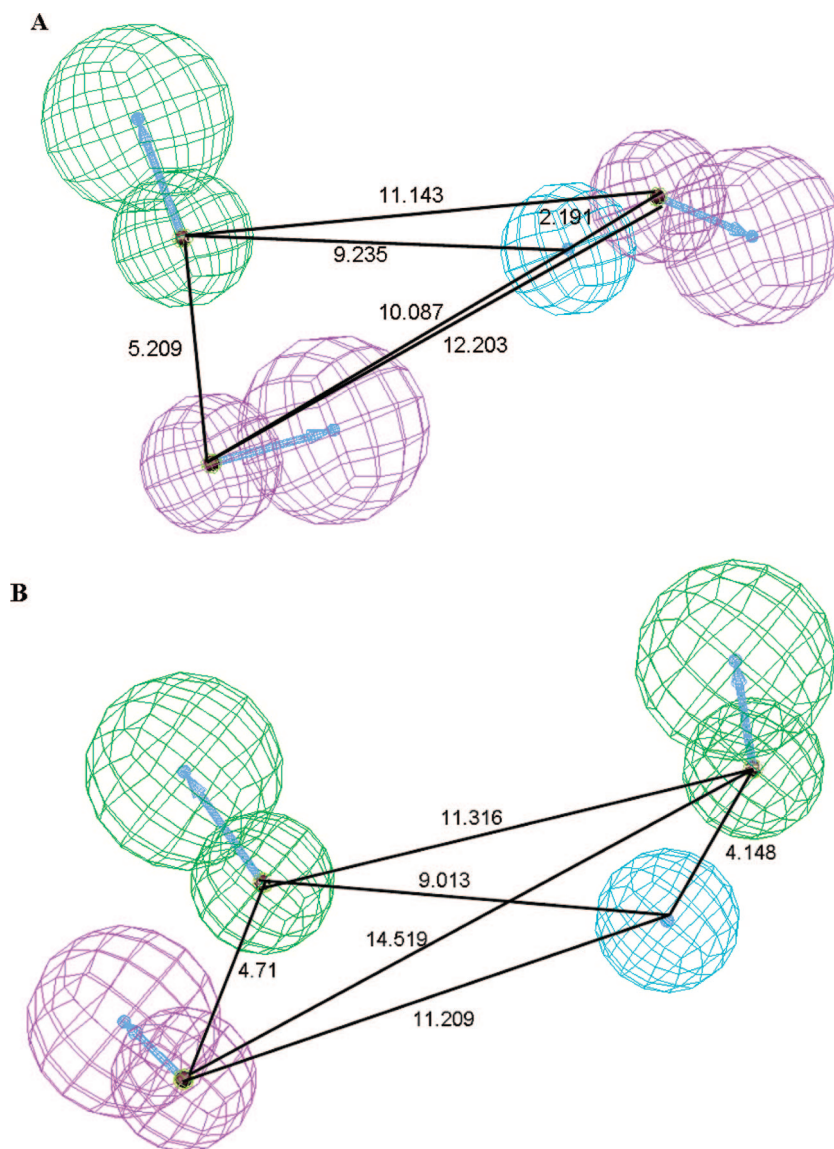
Figure 1. Best hypotheses models produced by the HypoGen module in Catalyst 4.11: (A) model of HypoA and (B) model of Hypo B. Pharmacophore features are color-coded with green, magenta, and cyan contours representing the hydrogen-bond acceptor, hydrogen-bond donor, and hydrophobic feature, respectively. The distance between pharmacophore features is reported in angstroms (Å).

An additional validation based on Fischer's randomization test using Cat. Scramble of CATALYST was conducted on the two hypotheses. In this test, the biological data and the corresponding structures are scrambled several times, and the software is challenged to generate pharmacophoric models from the randomized data. The confidence in the parent hypotheses (i.e., generated from unscrambled data) is lowered proportional to the number of times the software succeeds in generating binding hypotheses from scrambled data of apparently better cost criteria than the parent hypotheses. This approach minimizes the possibility of adopting fortuitous pharmacophores, which might happen because of the vast number of potential pharmacophores that CATALYST evaluates during a particular modeling cycle (up to 2;[17] see above). The costs of two hypotheses generated for the 99 randomized data sets was higher than that of 10 best hypothesis's costs (see Figure 1 in Supporting Information). This shows that our models are 99% statistically significant. The predictive power of the HypoA1 and HypoB1 was validated using a test set comprising of **50** compounds. The validation showed a good correlation between the

estimated and experimental data, with a correlation of 0.810 and 0.873 for HypoA1 and HypoB1, respectively (Figure 3A and B).

The combined features of the two high-quality pharmacophore models are complementing the binding pocket of MK2 receptor. Therefore, designing novel MK2 inhibitor compounds or virtual screening considering these combined features would provide better results.

2.2. Docking Studies. Docking studies using Glide (version 2.5) were performed for 77 carboline derivatives with MAPKAP2, having a PDB entry code 2PZY (2.9 Å). Preparation of the protein for docking included removal of ligand and solvent coupled with addition of hydrogen atoms. Standard Precision (SP) mode of Glide was used for the docking studies. The credibility of the docking method to predict the bioactive conformation was authenticated using the X-ray structure of MAPKAP2 in complex with a small molecule ligand, inhibitor **58**. Inhibitor **58** was docked into the active site of MAPKAP2, and the docked conformation having lowest docking energy was selected as the most probable binding conformation. The superposition of Glide

Table 1. Statistical Details of the Pharmacophore Models (HypoA and HypoB)

hypotheis no.	total cost	cost difference	error cost	rms	correlation (r)	features
			Hypothesis A			
1	102.832	141.959	86.594	0.77	0.975	HBA, HBD, HBD, HY
2	107.21	137.581	90.927	0.961	0.963	HBA, HBD, HBD, HY
3	115.282	129.509	98.976	1.232	0.963	HBA, HBD, HBD, HY
4	116.227	128.564	99.190	1.241	0.935	HBA, HBD, HBD, HY
5	116.515	128.276	100.033	1.266	0.932	HBA, HBD, HBD, HY
6	117.192	127.599	98.766	1.22	0.936	HBA, HBD, HBD, HY
7	117.222	127.569	101.02	1.294	0.929	HBA, HBD, HBD, HY
8	117.323	127.468	100.761	1.287	0.930	HBA, HBD, HBD, HY
9	117.874	126.917	99.109	1.239	0.935	HBA, HBD, HBD, HY
10	118.953	125.838	102.424	1.334	0.924	HBA, HBD, HBD, HY
			Null cost of 10 top-scored hypotheses is 244.791. Fixed cost value is 94.584. Configuration cost is 15.076			
			Hypothesis B			
1	104.144	121.515	86.192	0.760	0.973	HBA, HBA, HBD, HY
2	108.598	117.061	90.459	0.945	0.958	HBA, HBA, HBD, HY
3	110.640	115.019	92.360	1.101	0.951	HBA, HBD, HBD, HY
4	111.334	114.325	92.886	1.036	0.949	HBA, HBA, HBD, HY
5	111.593	114.066	92.220	1.0124	0.951	HBA, HBA, HBD, HY
6	113.065	112.594	94.819	1.103	0.942	HBA, HBD, HBD, HY
7	113.245	112.414	93.996	1.075	0.945	HBA, HBA, HBD, HY
8	113.400	112.259	93.635	1.062	0.946	HBA, HBA, HBD, HY
9	113.663	111.996	95.644	1.130	0.939	HBA, HBA, HBD, HY
10	113.663	111.996	94.662	1.098	0.943	HBA, HBA, HBD, HY
			Null cost of 10 top-scored hypotheses is 225.659. Fixed cost value is 96.070. Configuration cost is 16.563			

predicted conformation of inhibitor **58** with X-ray crystallographic ligand was shown in Figure 2 in Supporting Information. The root mean-square deviation (rmsd) between these two conformations was 1.13 Å, suggesting a high docking reliability of Glide in terms of reproducing the experimentally observed binding mode for MAPKAP2 inhibitors. All 77 inhibitors were docked into the active site of MAPKAP2, and the correlation was calculated between Glide score and the pIC_{50} by linear regression analysis method. An acceptable correlation coefficient (r) of 0.81 was obtained between experimental pIC_{50} and docking energy (Figure 3c). This correlation proved that the binding conformations and binding models of the carboline derivative inhibitors to MAPKAP2 are reliable, and this is further confirmed by the observation that high active compounds are having better glide scores than the low active compounds.

Our docking results disclosed that each of the compound is forming at least two hydrogen bond interactions with hinge region amino acids (exclusively with Met138 and Leu141) and with Asp207 and Lys93 of the receptor's binding site. The carboline ring which is present in every compound possessed hydrogen bond interactions with these amino acids. The compounds with high activity participated in more interactions, mainly, with Cys140, Asp142 (hinge amino acids), Leu70, Thr206, and Gly143. The large number of interactions in high actives is the result of the presence of a feature-rich substituent, amido thiazolyl carbomide. Thus the highly active compounds reflected there binding ability by having a minimum/maximum of three hydrogen bond interactions with hinge region of the binding site of MK2.

The non-bonded interactions between the most active compound (**67**) and amino acids of MK2 binding site are shown in the figure (Figure 4). As depicted from the figure, the receptor and ligand are tightly bound to each other by forming a network of hydrogen bond interactions. Among them the interactions observed with hinge region (Met138, Cys140, Leu141, and Asp142) amino acids are crucial for

the binding affinity. The binding forces between the compound and hinge region of MAPKAP2 are displayed as four hydrogen bond interactions: amino nitrogen at the ninth position of carboline ring forming a hydrogen bond interaction with sulfur of Met138 (S···HN, 2.72 Å); multicenter (bifurcated) hydrogen bond between the carbonyl O atom of amide group (between carboline and thiazoline rings), and NH of Glu139 (1.839 Å), also with SH of Cys140 (2.678 Å), and the SH of Cys140 also makes a hydrogen bond with the sulfur atom of thiazole ring (2.810 Å). The hydrogen bond interactions found outside of the hinge region are amino nitrogen at the second position of carboline ring establishing a hydrogen bond interaction with carboxyl oxygen atom of Lys93 (O···HN, 2.02 Å), the carboxyl O atom at the first position of carboline ring forming bifurcated hydrogen bond interactions with amino nitrogens of Asp207 (O···HN, 3.00 Å), and NH of Lys93 (2.56 Å).

The obtained pharmacophore models can be compared well with the docking interactions. The best docking pose of the high active compound **67** has a much lower rmsd (0.93 Å) value with the pharmacophore mapped conformation of this compound (Figure 5). The two HBAs of HypoB1 mapped to sulfur and oxygen containing moieties, thus complementing the hydrogen bond interactions with Lys140 and Asp207, respectively. The common HBD feature of the pharmacophore models, which is mapped to the amide group present between thiozole and piperdine rings augment the interaction with Asp142. One of the hydrogen bond donors that is absent in HypoB1 and mapped in HypoA1 appeared to be an important feature affecting the activity because its counterpart in docking is represented by the hydrogen bond interaction with Lys93.

2.3. COMFA and COMSIA Studies. From the total set of 77 carboline derivatives, only 54 compounds having specific activity for MAPKAP2 were chosen for developing CoMFA and CoMSIA models. A training set of 42 compounds was used for models generation. An external test set
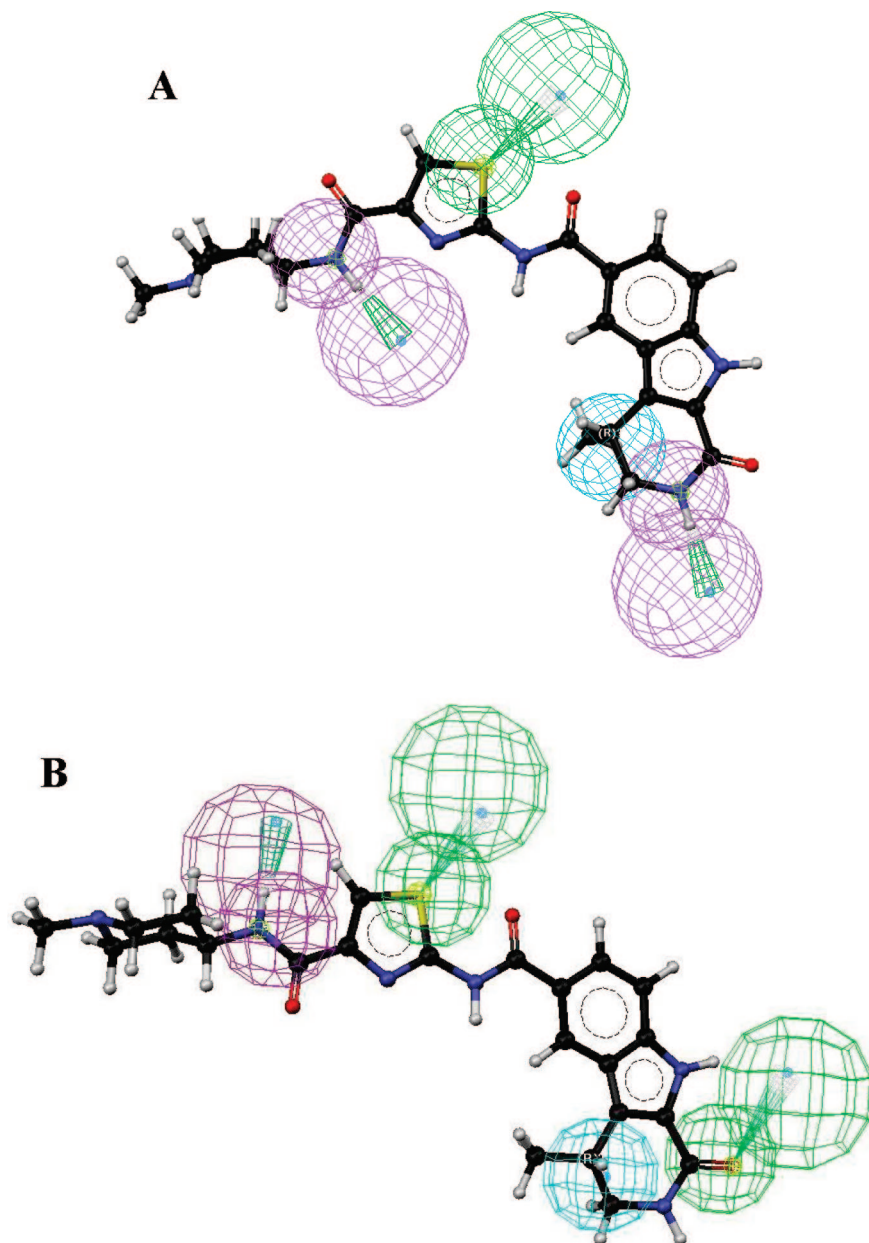
Figure 2. Pharmacophore mapping of the most active compound **67** on the best hypotheses models: (A) high active compound **67** with HypoA and (B) with HypoB.

of 12 compounds having chemical diversity and covering all ranges of activity was used to assess the exactness of the models generated. The leave-one-out and leave-five-out partial least-squares (PLS) analyses of the obtained models yielded excellent cross-validated q^2 and r^2_{LFO} values of 0.804 and 0.852 with five components, respectively. Because the cross-validated correlation coefficient (q^2) is used as a measure of reliability of prediction, these correlation coefficients suggest that our model is reliable and accurate. Subsequently, internal noncross-validated PLS regressions were computed using the previously obtained optimum number of components giving regression coefficient r^2 of 0.984 with a standard error of estimate (SEE) of 0.119. The conventional correlation coefficient indicates the goodness of the fit of QSAR model. The predicted pIC$_{50}$ values for each training set of compounds are given in Table 2.The statistical parameters associated with all the models are shown in Table 3. Figure 3D shows the relationship between

the CoMFA-predicted and experimental pIC$_{50}$ values of the non cross-validated analyses for carboline derivatives.

CoMSIA is an alternative molecular field analysis method to CoMFA. It is thought to be less affected by changes in molecular alignment and provides smoother and interpretable contour maps as a result of employing Gaussian type distance dependence with the molecular similarity indices. CoMSIA models were generated using the combinations of the following descriptor fields: steric, electrostatic, hydrophobic, H-bond donor and H-bond acceptor. These descriptors illustrate various properties into spatial locations where they play a decisive role in determining the biological activity. The statistical details of CoMSIA model are summarized in Table 3. The combined use of all the six/five descriptors resulted in the best model with $q^2 = 0.765$, $r^2_{LFO} = 0.801$, and $r^2 = 0.986$ (six components), respectively. Final predicted/cross-validated versus experimental pIC$_{50}$ values for models and their residuals are given in Table 3. Figure
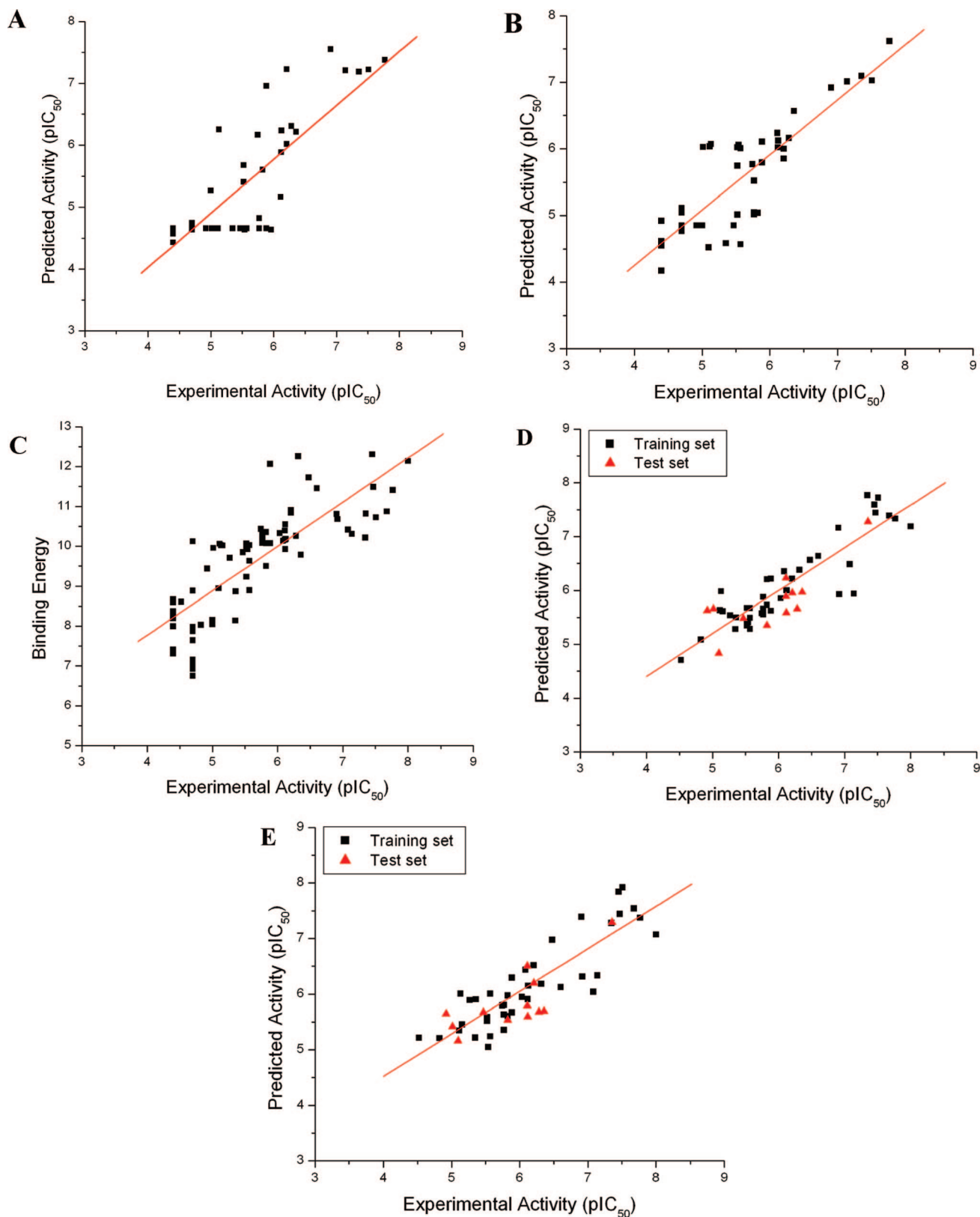
Figure 3. (A) Plot of experimental versus predicted pIC_{50} for hypo A model. (B) Plot of experimental versus predicted pIC_{50} for hypo B model. (C) Plot showing correlation between experimental activity and glide docking score. (D) Plot of experimental versus predicted pIC_{50} for CoMFA model. (E) Plot of experimental versus predicted pIC_{50} for CoMSIA model.

4E shows the experimental activities versus predicted ones in the training and test sets by CoMSIA models, respectively.

2.4. Validation of QSAR Models. The validation of the QSAR models, which very well reproduced the experimental activity for the training set, was done to verify the excellent

statistical parameters/correlations that were observed and also to investigate whether the activity of carboline derivatives can be predicted well with these models. The ultimate test for the predictability of a QSAR analysis in the drug design process is the ability of the model to predict the biological

INHIBITORS OF MAPKAP K2

J. Chem. Inf. Model., Vol. 49, No. 1, 2009 **59**
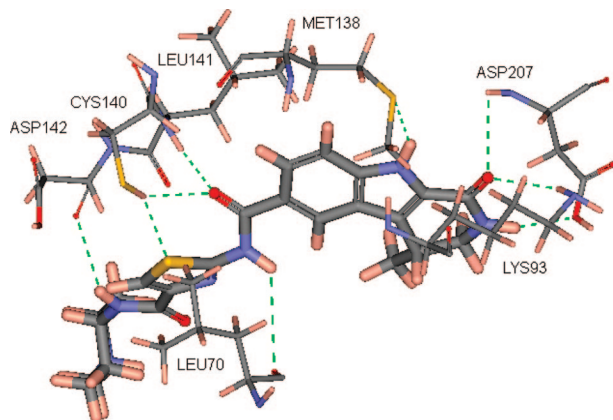
Figure 4. H-bond interactions between the hinge region of MAPKAP K2 and high active compound **67**.
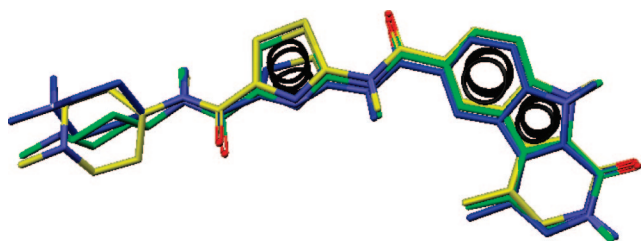
Figure 5. Superimposition of pharmacophore models (HypoA and HypoB) and the binding conformation of high active compound **67**. The HypoA conformation is in yellow; the HypoB conformation is in green, and binding conformation is in blue.

activity of compounds that have not been included in the training set. The predicted versus the experimental selectivity values for the training and the test sets are depicted in Figure 4. Correlation between the experimental and predicted activities was calculated for the test set compounds (r_{pred}^2) according to the formula of Cramer et al.[32] The predictive power of the CoMFA model ($r_{pred}^2 = 0.931$) was better than that of CoMSIA model ($r_{pred}^2 = 0.921$). Overall, our models exhibited very high preciseness both in regular cross validation and in the prediction of activity of test set molecules.

2.5. 3D Contour Map Analyses. Contour maps were produced to envision the information content of the derived 3D-QSAR, CoMFA, and CoMSIA models. The field energies at each lattice point were calculated as the scalar results of the coefficient and the standard deviation associated with a particular column of the data table (stdev*coeff) was plotted as the percentage of the contribution to the CoMFA or CoMSIA equation. In Figures 6–9, the isocontour diagrams of the field contributions (stdev*coeff) for different properties calculated by the CoMFA and CoMSIA analysis are illustrated with exemplary ligands. Selectivity fields depict the change in the binding preference occurring depending upon the variation in the molecular fields around ligands. The contour plots help in identifying the important regions where any change will subsequently may affect the binding preference. Furthermore, they would be helpful in establishing the important features (pharmacophore) contributing to activity and relating them with interactions between the ligand and the active site of a receptor.

2.5.1. CoMFA Contours. The steric properties derived from the carboline inhibitory activity data using CoMFA is displayed in the Figure 6A and B. The areas indicated by green contours correspond to regions, where occupancy with

steric bulky groups should increase the activity. In contrast, occupation of the areas encompassed by yellow isopleths by steric groups should be avoided because reduced activity can be expected otherwise. As depicted in Figure 6, the carboline derivative **67** (highest active ligand) orients its thiazole and methyl-piperidine rings to the green contours, while among the lowest active compounds, the orientation of its substituents projects toward yellow region. Accordingly, the methoxy groups of **70** and **1**, the halogen of **5**, the acetamide groups of **9** and **10**, and the ortho- and meta-substituted phenyl acetamido groups of **26**, **29**, **37**, **38**, and **39** are pointing toward the lowered activity representing yellow isopleths. The compounds with long chains substituted at the fifth position of the thiazole ring have lowered activity (**54**, **55**, **68**, **69**) compared to those that have substitutions at fourth position (**52**, **53**, **58**, **60**) because the former groups are oriented on to this yellow region. This may be caused by steric repulsions/hindrances. In addition, the upper yellow map near the para-position of phenyl acetamido moieties of **40**, **41**, and **43**−**46** indicates that the presence of bulky substituents in this region decreases kinase inhibitory activity. The appearance of green contour near R2 position indicates that bulkier groups are favored at this position. In case of compounds **70**, **72**, and **1**, the presence of bulkier moieties at this position corresponded with increments in the activity profile.

In Figure 6C and D, the electrostatic property maps are illustrated for the molecules **67** and **70** as examples for high and low activity ligands, respectively. The blue areas above and below the 2-cetamido-thiozole group reflect a common placement of this function within the highly active ligands. The red areas are positioned in the vicinity of the carboxylic group of thiazole-4-carboxylic acid amide of highly active ligands.

2.5.2. CoMSIA Contours. In Figure 7A and B, the steric properties derived from the MAPKAP activity data for CoMSIA are displayed. As depicted, the two green and one yellow areas of CoMSIA steric map can be well compared with the steric contour maps of CoMFA. It signifies that these isopleths are essentially required for the hydrophobic interactions with the receptor's active site amino acids. The electrostatic contour map (Figure 7C and D) of CoMSIA has a small variation with that of CoMFA. The red and blue contours appearing near electron rich carbonyl oxygen and protonated secondary amine nitrogen of amido thiazole ring reveals the significance of arrangement of electronegative and electropositive groups at these positions, respectively. The demonstrated significance is evident from the maps, by the presence of blue contour in the vicinity of nitrogen atom of amide group positioned in between thiazole and piperzine ring of all the highly active compounds (**53**, **56**, **58**−**60**, **62**−**65**, **67**). Correspondingly, compounds lacking protonated nitrogen at this position were showing reduced activity (**66**, **57**). In addition, the red map near the electron-rich, tertiary nitrogen (N2) of piperazine ring suggests that the position specific occurrence of electronegative groups increases the MAPK kinase inhibitory activity.

Figure 8A and B depicts the contour plot of the hydrogen bond acceptor field contributions to the activity obtained for the CoMSIA model. As depicted, a large hydrogen bond acceptor (red) area surrounds the substituent portion of the carboline scaffold of compound **67**. The presence of two

Table 2. Structures of Carboline Analogs, Their Experimental, QSAR, and Pharmacophore Predicted Activities with Docking Energies
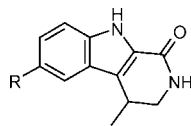
Compound	R	pIC_{50}	CoMFA Predicted (pIC_{50})	CoMSIA Predicted (pIC_{50})	Pharmacophore Predicted IC_{50} (µm)	Docking energy
1	OMe	5.350	5.281	5.222	4.585	-8.140
2	H	4.397	--	--	4.568	-7.995
3	Me	4.397	--	--	4.568	-7.313
4	Ph	4.397	--	--	4.585	-8.638
5	Br	4.823	5.088	5.21	4.585[b]	-8.034
6	OH	4.397	--	--	4.568	-8.199
7		4.397	--	--	4.619	-8.669
8		4.397	--	--	4.920	-7.411
9		5.267	5.537	5.893	4.853[b]	-9.706
10		4.920	5.627[a]	5.643[a]	4.853	-9.437
11		4.698	--	--	4.823	-7.649
12		4.698	--	--	4.769	-7.982
13		4.698	--	--	4.853[b]	-7.160
14		5.537	5.401	5.051	6.060	-9.928
15		4.698	--	--	4.853	-7.963
16		4.698	--	--	5[b]	-6.754
17		6.283	5.66[a]	5.677[a]	6.161	-10.257
18		6.119	5.583[a]	5.594[a]	6.022	-9.929
19		6.086	6.354	6.436	6.229[b]	-10.132
20		5.823	5.351[a]	5.532[a]	5.744[b]	-10.074
21		5.823	5.73	5.606	5.040	-9.503
22		6.356	5.964[a]	5.693[a]	6.568	-9.788
23		4.698	--	--	4.823[b]	-8.888
24		5.823	6.206	5.972	5.958[b]	-10.354
25		4.698	--	--	4.853	-7.872

Table 2. Continued
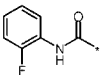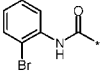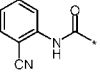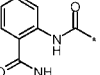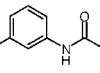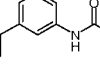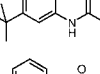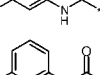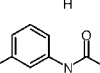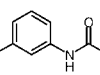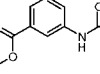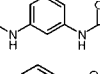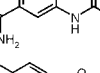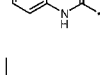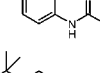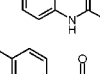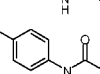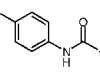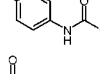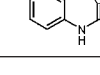
Compound	R	pIC_{50}	CoMFA Predicted (pIC_{50})	CoMSIA Predicted (pIC_{50})	Pharmacophore Predicted IC_{50} (μm)	Docking energy
26		5.013	5.658[a]	5.416[a]	6.026	-9.959
27		5.000	--	--	4.853	-8.045
28		5.000	--	--	5.397[b]	-8.157
29		5.522	5.414	5.591	5.744	-9.231
30		5.468	5.468[a]	5.673[a]	4.853	-9.846
31		4.698	--	--	5.113	-7.038
32		4.698	--	--	4.853	-6.926
33		5.769	5.658	5.633	5.049	-10.304
34		5.886	5.623	5.672	5.795	-10.077
35		5.568	5.67	6.009	6.008	-10.027
36		6.113	5.884[a]	5.791[a]	6.236	-10.163
37		5.130	5.985	6.006	6.070	-10.025
38		5.356	5.499	5.905	5.677[b]	-8.871
39		5.568	5.492	6.006	5.853[b]	-9.633
40		5.522	5.351	5.523	6.022	-9.987
41		5.113	5.632	5.348	6.036	-10.062
42		4.698	--	--	5.045	-10.121
43		5.522	5.676	5.538	5.013	-10.064
44		5.769	5.555	5.359	5.017	-10.081
45		5.154	5.612	5.455	4.958[b]	-10.018
46		5.769	5.878	5.803	5.522	-10.197
47		6.031	5.852	5.947	5.795[b]	-10.326

Table 2. Continued

Compound	R	pIC$_{50}$	CoMFA Predicted (pIC$_{50}$)	CoMSIA Predicted (pIC$_{50}$)	Pharmacophore Predicted IC$_{50}$ (µm)	Docking energy
48		5.744	5.576	5.796	5.769	-10.433
49		6.207	5.95[a]	6.193[a]	5.823	-10.909
50		6.119	6.004	5.906	5.958[b]	-10.545
51		6.207	6.217	6.517	6	-10.839
52		6.124	5.998	6.148	6.124	-10.181
53		7.080	6.486	6.039	7.180[b]	-10.414
54		6.113	6.231[a]	6.502[g]	6.136[b]	-10.395
55		6.920	5.929	6.316	6.697[b]	-10.682
56		7.142	5.937	6.333	7.013	-10.309
57		6.477	6.565	6.977	6.036[b]	-11.729
58		7.468	7.455	7.44	7.721[b]	-11.490
59		7.769	7.334	7.374	7.619	-11.410
60		7.455	7.594	7.842	7.387[b]	-12.305
61		6.906	7.163	7.391	6.920	-10.809
62		7.677	7.387	7.54	7.60[b]	-10.875
63		7.508	7.721	7.922	7.026	-10.724
64		7.346	7.769	7.28	7.214[b]	-10.215
65		7.356	7.277[a]	7.292[g]	7.096	-10.821
66		6.602	6.64	6.123	6.229[b]	-11.452
67		8.000	7.19	7.071	7.154[b]	-12.141
68		5.886	6.218	6.294	6.107	-12.064
69		6.318	6.38	6.184	6.292[b]	-12.260

Table 2. Continued

Compound	R	pIC$_{50}$	CoMFA Predicted (pIC$_{50}$)	CoMSIA Predicted (pIC$_{50}$)	Pharmacophore Predicted IC$_{50}$ (µm)	Docking energy
70*		4.522	4.708	5.217	4.585[b]	-8.603
71*		5.096	4.829[a]	5.159[a]	4.522	-8.944
72*		5.568	5.285	5.243	4.568	-8.893
73*		4.397	--	--	4.173	-6.360
74*		4.397	--	--	4.602	-7.991
75*		4.397	--	--	4.552	-7.599
76*		4.397	--	--	4.619[b]	-7.374
77*		4.397	--	--	4.619	-6.269

* Compounds from 70 to 77 are full structures. [a] Compounds included in test set for CoMFA and CoMSIA. [b] Compounds included in training set for pharmacophore studies.

Table 3. Summary of CoMFA and CoMSIA Model Result[a]

| component	CoMFA	CoMSIA
q^2	0.804	0.765
r^2	0.984	0.986
n	5	6
r^2_{pred}	0.931	0.921
r^2_{LFO}	0.852	0.801
F value	436.553	424.287
SEE	0.119	0.111
steric	38.7%	14.0%
electrostatic	61.3%	26.3%
donor		17.9%
acceptor		17.8%
hydrophobic		23.9%

[a] q^2, LOO cross-validated correlation coefficient; r^2, non-cross validated correlation coefficient; n, number of components used in the PLS analysis; r^2_{pred}, predictive correlation coefficient; r^2_{LFO} leave five out cross validated predictive correlation coefficient; F value, F-statistic for the analysis; SEE, standard error of estimate.

amide oxygens and electron-rich atoms (nitrogen and sulfur) of electrocyclic rings in substituents of all the highly active compounds are the reasons for this large acceptor region. These electron-rich atoms were also found to have critical interactions with hinge region amino acids in the docking studies (Figure 4). As depicted in Figure 4, the sulfur and oxygen atoms of 2-acetamido-thiozole group, identified as a hydrogen bond acceptors, interact with the side-chain SH

moiety of the Cys140 residue and amide proton of Leu141, respectively. Both the pharmacophore models that were discussed earlier in this study identified the sulfur atom as an acceptor. The hydrophobic maps (Figure 9A and B) are similar to steric maps of CoMSIA. The graphical interpretation of the field contributions of the H-bond donor (from CoMSIA) is shown in Figure 8C and D. Cyan contour maps define that a H-bond donor group within a ligand will be advantageous for the binding preference toward the MAPK kinase receptor, while purple isopleths represent unfavorable regions of H-bond donors. For the highest active compound **67**, the cyan area is visible near the protonated nitrogen's of the amide group present in between thiozole and piperdine rings. The presence of hydrogen bond donor groups like primary and secondary amines at this position will raise the inhibitory activity. Constitutively, compounds **53** and **56** having a primary and a secondary amine at these positions showed greater activity than the compounds (**57, 66**) bearing a tertiary amine. Furthermore, our docking studies revealed that these primary and secondary amines that are present in the highly active compounds act as hydrogen bond donors and form strong hydrogen bond interactions with main chain CO of Leu70 (Figure 4). The QSAR analysis also picked it as an important hydrogen bond donor feature in both the pharmacophore models.
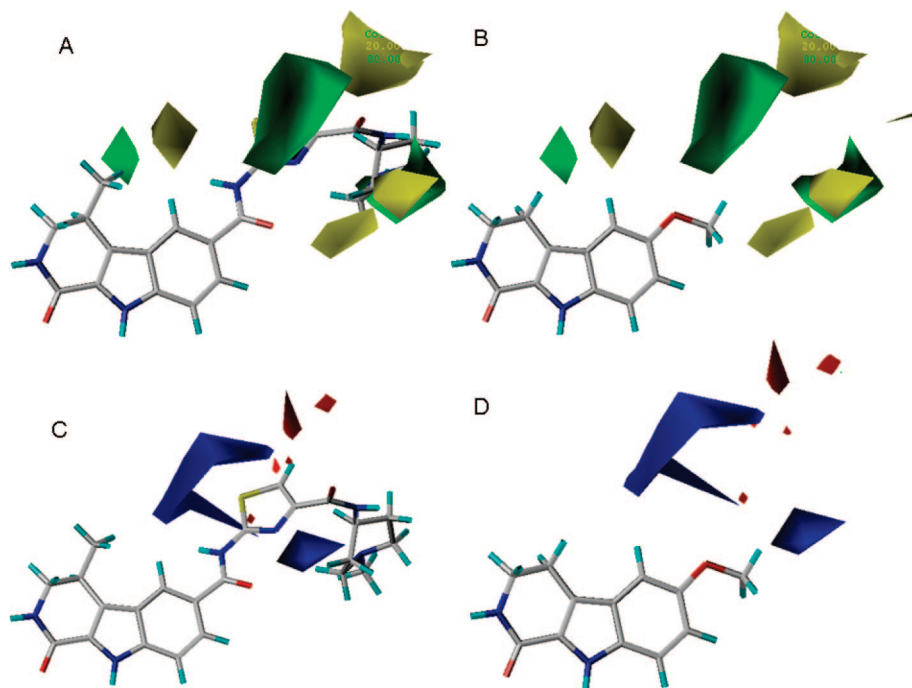
Figure 6. CoMFA contour maps for MAPKAP K2 inhibitors: (A) the steric maps for high active compound **67** and (B) for low active compound **70** and (C) the electrostatic maps for high active compound **67** and (D) for low active compound **70**. Green contour maps represent sterically favored areas, and sterically disfavored areas are in yellow. Positive potential favored areas are in blue; negative potential favored areas are in red.
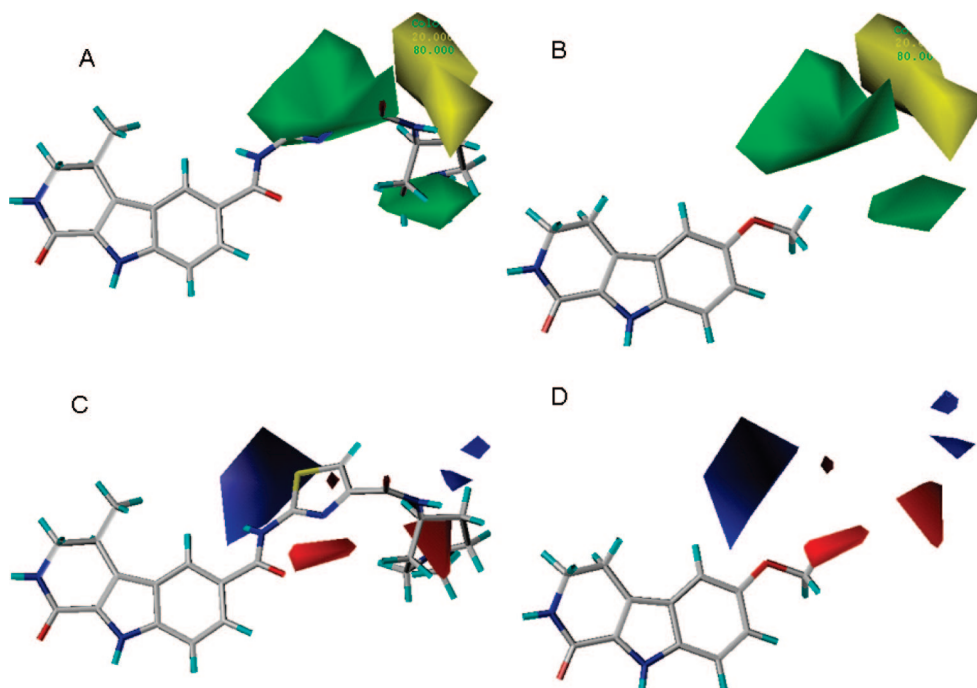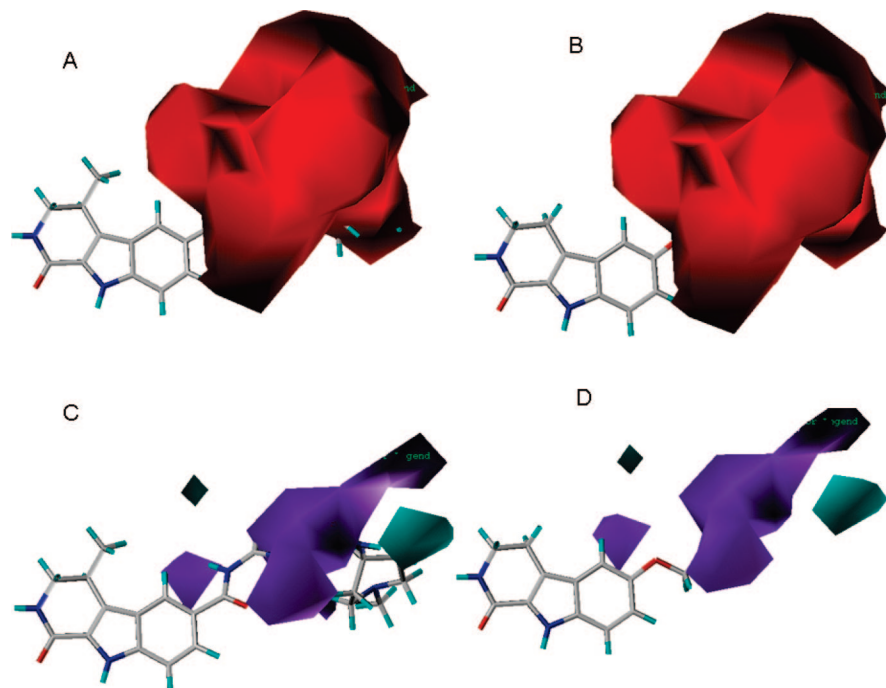

Figure 7. CoMSIA contour maps for MAPKAP K2 inhibitors: (A) the steric maps for high active compound **67** and (B) for low active compound **70** and (C) the electrostatic maps for high active compound **67** and (D) for low active compound **70**.

3. CONCLUSIONS

Our results suggest that pharmacophore modeling of MK2 can be a useful tool for finding potential anti-inflammatory agents. The exploration of the pharmacophoric space using CATALYST-HYPOGEN was performed to identify the two complementary models against binding site of the receptor. Pharmacophore studies suggests that two hydrogen bond acceptors, two hydrogen bond donors, and one hydrophobic feature is essential for ligand binding, and it was proven by

the docking studies where these features are well complemented with the interacting aminoacids, Leu70, Lys93, Asp207, Cys140, and Leu141 in the binding site of MK2.The 3D QSAR models described herein possesses a good internal and external consistency. The good correlation between experimental and predicted pIC_{50} values for the test compounds further proved the predictive power of the constructed QSAR model. CoMFA and CoMSIA contour maps, which are shown in 3D spaces are useful in guiding the suitable

Figure 8. CoMSIA contour maps for MAPKAP K2 inhibitors: (A) the H-bond acceptor maps for high active compound **67** and (B) for low active compound **70** and (C) the H-bond donor maps for high active compound **67** and (D) for low active compound **70**. The red contour for H-bond acceptor group increase activity, whereas the cyan contour for the H-bond donor indicates the favored region, and purple indicates the disfavored region.
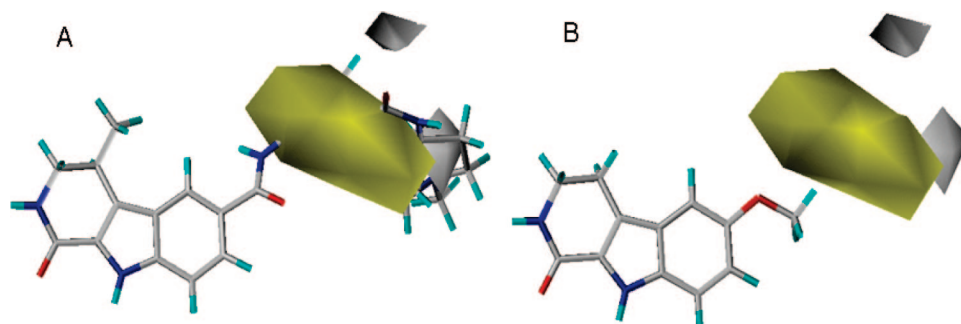
Figure 9. CoMSIA contour maps for MAPKAP K2 inhibitors: (A) the hydrophobic maps for high active compound **67** and (B) for low active compound **70**. The yellow contour indicates the hydrophobic favored region; white indicates the hydrophilic favored region.

structural modifications of the compound for showing higher biological activity. Moreover, the 3D QSAR model generated is compatible with the 3D protein environment in the MK2 binding site, suggesting possible synergism between QSAR and structure-based technologies. Integration of these experiments results will provide the knowledge required for better understanding of structural features necessary for biological interaction. In addition, these studies will also furnish information on the common and diversified chemical features forming the components of inhibitors, responsible for the altered activity, and forms a basis for further modification focusing the improved potency of the molecules.

4. MOLECULAR MODELING

4.1. Data Set. The three-dimensional structures were constructed using SYBYL programming package, version 6.7.[28] The published inhibitory activities (IC$_{50}$) against MK2 were used as dependent variables in the QSAR study.[27] Energy minimization was performed using Tripos force field,[29] the Gasteiger–Huckel[30] charge with a distance-dependent dielectric, and Powell conjugate gradient algorithm with convergence criterion of 0.05 kcal/mol. Further geo-

metric optimization of these compounds was done using the semiempirical program MOPAC 6.0 and applying the AM1 Hamiltonian.[31]

4.2. QSAR Studies. QSAR modeling (CoMFA, Co-MSIA)[32−34] concerns the extraction of a quantitative relationship between the experimentally observed biological activity of a set of compounds and a number of descriptors related to physical, chemical, and structural properties of the compounds. The 54 molecules in QSAR data set were divided into a training set of 42 compounds and a test set with 12 compounds. A satisfactory QSAR relation was generated by using the partial least squares (PLS)[35] as the fitting technique to weigh the relative contribution of each descriptor in the final model. PLS has proven superiority in handling data with strong correlation and having numerous independent variables. PLS, in particular, is able to identify linear combinations of the original physicochemical descriptors that are better for correlating the data thereby providing statistically more robust solutions.[36] Once the equation derived, the equation was tested against the test set.

4.3. Pharmacophore Modeling. In this study, the Catalyst 4.10[37] software package was applied for automated ligand-

based pharmacophore generation. Multiple acceptable conformations were generated for all ligands using the Poling algorithm.[38] A maximum of 250 conformations were generated for each molecule within an energy threshold of 20.00 kcal/mol above the global energy minimum. The training set molecules (27) associated with their conformations was submitted to the Catalyst hypothesis generation (HypoGen) using default uncertainty value 3. Features such as hydrogen-bond acceptor, donor, and hydrophobic were included for the pharmacophore generation on the basis of common features present in the study molecules. The 3D pharmacophore models called "hypotheses" were derived from training set. The training set molecules were carefully chosen with respect to discrepancy in structure and biological activity among all the compounds. A set of 50 molecules, which were not included in training set, was considered as a test set. The best Pharmacophore models (HypoA1, HypoB1) with high correlation coefficients (*r*) and the lowest rmsd values were chosen to estimate the activity of test set.

4.3.1. Pharmacophore Validation. The derived pharmacophore map was validated using cost analysis, test set prediction, and enrichment factor. The HypoGen module in catalyst performs two important theoretical cost calculations (represented in bit calculations). One is the "fixed cost" (ideal cost), which represents model that fits all data perfectly, and the second is "null cost" (correlation cost), which represents the highest cost of a pharmacophore with no features and estimate activity to be the average of the activity data of the training set molecules. The difference of 40−60 bits between null and fixed cost may indicate that it has 75−90% probability of correlating the data.

The total cost of any pharmacophore hypothesis should be close to the fixed cost to provide any useful models. Two other parameters that also determine the quality of any pharmacophore hypothesis are configuration cost, which should have a value of <17, and the error cost, which is dependent on the root-mean-square differences between the estimated and actual activities of the training set molecules. The best pharmacophore model has highest cost difference, lowest rmsd, and best correlation coefficient.

4.4. Docking. For the docking of ligands into protein active site and for estimating the binding affinities of docked compounds, we used an advanced molecular docking program Glide, version 2.5,[39] in this study. During the docking process, initially Glide performs a complete systematic search of the conformational, orientational, and positional space of the docked ligand and eliminates unwanted conformations using scoring and followed by energy optimization. Finally, the conformations are further refined via a Monte Carlo sampling of pose conformation. Prediction of the binding affinity and rank-ordering ligands in database screens was implemented by modified and expanded version of the ChemScore18 scoring function, Glide Score. For our studies, X-ray crystal structure of MK2 kinase was taken from PDB (2PZY) and has a resolution of 2.90 Å. The performance of the docking method was evaluated by redocking crystal ligand and correlating the docking scores with activity of the carboline derivatives.

Supporting Information Available: Figures showing the Catscramle graph for (A) HypoA and (B) HypoB using 49 randomized sets and the superimposition of crystal ligand

and glide docked conformation for compound **58**. This material is available free of charge via the Internet at http://pubs.acs.org.

REFERENCES AND NOTES

(1) Noble, M. E.; Endicott, J. A.; Johnson, L. N. Protein kinase inhibitors: Insights into drug design from structure. *Science* **2004**, *303*, 1800–1805.

(2) Schäfer, M.; Egner, U. Structural aspects of drugability and selectivity of protein kinases in inflammation. *Anti-Inflammatory Anti-Allergy Agents Med. Chem* **2007**, *6*, 5–17.

(3) Ono, K.; Han, J. The p38 signal transduction pathway: activation and function. *Cell Signaling* **2000**, *12*, 1–13.

(4) Lee, J. C.; Kassis, S.; Kumar, S.; Badger, A.; Adams, J. L. Pyrimidinylimidazole inhibitors of p38: Cyclic N-1 imidazole substituents enhance p38 kinase inhibition and oral activity. *Pharmacol. Ther.* **1999**, *82*, 389–397.

(5) Lu, H. T.; Yang, D. D.; Wysk, M.; Gatti, E.; Mellman, I.; Davis, R. J.; Flavell, R. A. Defective IL-12 production in mitogen-activated protein (MAP) kinase kinase 3 (MKK3)-deficient mice. *EMBO J.* **1999**, *18*, 1845–1857.

(6) Wysk, M.; Yang, D. D.; Lu, H. T.; Flavell, R. A.; Davis, R. J. Requirement of mitogen-activated protein kinase kinase 3 (MKK3) for tumor necrosis factor-induced cytokine expression. *Proc.Natl. Acad. Sci. U.S.A.* **1999**, *96*, 3763–3768.

(7) tokoe, D.; Caudwell, F. B.; Cohen, P. T. W.; Cohen, P. A. Comparison of the substrate specificity of MAPKAP kinase-2 and MAPKAP kinase-3 and their activation by cytokines and cellular stress. *J. Biochem.* **1993**, *296*, 843–849.

(8) Kotlyarov, A.; Neininger, A.; Schubert, C.; Eckert, R.; Birchmeier, C.; Volk, H. D.; Gaestel, M. MAPKAP kinase 2 is essential for LPS-induced TNF-alpha biosynthesis. *Nat. Cell Biol.* **1999**, *1*, 94–97.

(9) Stokoe, D.; Campbell, D. G.; Nakielny, S.; Hidaka, H.; Leevers, S. J.; Marshall, C.; Cohen, P. MAPKAP kinase-2: A novel protein kinase activated by mitogen-activated protein kinase. *EMBO J.* **1992**, *11*, 3985–3994.

(10) Rouse, J.; Cohen, P.; Trigon, S.; Morange, M.; Alonso-Llamazares, A.; Zamanillo, D.; Hunt, T.; Nebreda, A. R. A novel kinase cascade triggered by stress and heat shock that stimulates MAPKAP kinase-2 and phosphorylation of the small heat shock proteins. *Cell* **1994**, *78*, 1027–1037.

(11) Winzen, R.; Kracht, M.; Ritter, B.; Wilhelm, A.; Chen, C. Y. A.; Shyu, A.-B.; Muller, M.; Gaestel, M.; Resch, K.; Holtmann, H. The p38 MAP kinase pathway signals for cytokine-induced mRNA stabilization via MAP kinase-activated protein kinase 2 and an AU rich region-targeted mechanism. *EMBO J.* **1999**, *18*, 4969–4980.

(12) Han, J.; Lee, J. D.; Bibbs, L.; Ulevitch, R. J. A MAP kinase targeted by endotoxin and hypersmolarity in mammalian cells. *Science* **1994**, *265*, 808–811.

(13) Freshney, N. W.; Rawlinson, L.; Guesdon, F.; Jones, E.; Cowley, S.; Hsuan, J.; Saklatvala, J. Interleukin-1 activates a novel protein kinase cascade that results in the phosphorylation of Hsp27. *Cell* **1994**, *78*, 1039–1049.

(14) Rouse, J.; Cohen, P.; Trigon, S.; Morange, M.; Alonso-Llamazares, A.; Zamanillo, D.; Hunt, T.; Nebreda, A. R. A novel kinase cascade triggered by stress and heat shock that stimulates MAPKAP kinase-2 and phosphorylation of the small heat shock proteins. *Cell* **1994**, *78*, 1027–1037.

(15) Lee, J. C.; Laydon, J. T.; McDonnell, P. C.; Gallagher, T. F.; Kumar, S.; Green, D.; McNulty, D.; Blumenthal, M. J.; Heys, R. J.; Landvatter, S. W.; Strickler, J. E.; McLaughlin, M. M.; Siemens, I. R.; Fisher, S. M.; Livi, G. P.; White, J. R.; Adams, J. L.; Young, P. R. A protein kinase involved in the regulation of inflammatory cytokine biosynthesis. *Nature* **1994**, *372*, 739–746.

(16) Zervos, A. S.; Faccio, L.; Gatto, J. P.; Kyriakis, J. M.; Brent, R. Mxi2, a mitogen-activated protein kinase that recognizes and phosphorylates Max protein. *Proc. Natl. Acad. Sci. U.S.A.* **1995**, *92*, 10531–10534.

(17) Gaestel, M. MAPKAP kinases-MKs-two's company, three's a crowd. *Nat. Rev. Mol. Cell Biol.* **2006**, *7*, 120–130.

(18) Hannigan, M. O.; Zhan, L.; Ai, Y.; Kotlyarov, A.; Gaestel, M.; Huang, C. K. Abnormal migration phenotype of mitogen-activated protein kinase-activated protein kinase 2 neutrophils in Zigmond chambers containing formylmethionyl-leucyl-phenylalanine gradients. *J. Immunol.* **2001**, *167*, 3953–3961.

(19) Neininger, A.; Kontoyiannis, D.; Kotlyarov, A.; Winzen, R.; Eckert, R.; Volk, H. D.; Holtmann, H.; Kollias, G.; Gaestel, M. MK2 targets AU-rich elements and regulates biosynthesis of tumor necrosis factor and interleukin-6 independently at different post-transcriptional levels. *J. Biol. Chem.* **2002**, *277*, 3065–3068.

(20) (a) Klinkhoff, A. Biological agents for rheumatoid arthritis: targeting both physical function and structural damage. *Drugs* **2004**, *64*, 1267–

1283. (b) Barry, J.; Kirby, B. Novel biologic therapies for psoriasis. *Expert Opin. Biol. Ther* **2004**, *4*, 975–987.

(21) Stokoe, D.; Caudwell, F. B.; Cohen, P. T. W.; Cohen, P. The substrate specificity and structure of mitogen-activated protein (MAP) kinase-activated protein kinase-2. *Biochem. J.* **1993**, *296*, 843–849.

(22) Ben-Levy, R.; Leighton, I. A.; Doza, Y. N.; Attwood, P.; Morrice, N.; Marshall, C. J.; Cohen, P. Identification of novel phosphorylation sites required for activation of MAPKAP kinase-2. *EMBO J.* **1995**, *14*, 5920–5930.

(23) Clark, D. E. What has computer-aided molecular design ever done for drug discovery. *Expert Opin. Drug Discovery* **2006**, *1*, 103–110.

(24) Jalaie, M.; Erickson, J. Homology model directed alignment selection for comparative molecular field analysis: Application to photosystem II inhibitors. *J. Comput.-Aided Mol. Des.* **2000**, *14*, 181–197.

(25) Evers, A.; Gohlke, H.; Klebe, G. Ligand-supported homology modeling of protein binding-sites using knowledge-based potentials. *J. Mol. Biol.* **2003**, *334*, 327–345.

(26) Tafi, A.; Bernardini, C.; Botta, M.; Corelli, F.; Andreini, M.; Martinelli, A.; Ortore, G.; Baraldi, P. G.; Fruttarolo, F.; Borea, P. A.; Tuccinardi, T. Pharmacophore based receptor modeling: The case of adenosine A3 receptor antagonists. *J. Med. Chem.* **2006**, *49*, 4085–4097.

(27) Jiang-Ping, W.; Wang, J.; Abeywardane, A.; Andersen, D.; Emmanuel, M.; Gautschi, E.; Goldberg, D. R.; Kashem, M. A.; Lukas, S.; Wang, M.; Martin, L.; Morwick, T.; Moss, N.; Pargellis, C.; Usha, R. P.; Patnaude, L.; Gregory, W. P.; Donna, S.; Roger, J. S.; Yancey, W.; Werneburg, B.; Andre, W. The discovery of carboline analogs as potent MAPKAP-K2 inhibitors. *Bioorg. Med. Chem. Lett.* **2007**, *17*, 4664–4669.

(28) *SYBYL*, version 6.8; Tripos Associates: St. Louis, MO, 2000.

(29) Clark, M.; Cramer, R. D., III; Opdenbosch, N. V. Validation of the general purpose Tripos 5.2 force field. *J. Comput. Chem.* **1989**, *10*, 982–1012.

(30) Gasteiger, J.; Marsilli, M. Iterative partial equalization of orbital electronegativity—A rapid access to atomic charges. *Tetrahedron* **1980**, *36*, 3219–3228.

(31) Stewart, J. J. MOPAC: A semi empirical molecular orbital program. *J. Comput.-Aided Mol. Des.* **1990**, *4*, 1–103.

(32) Cramer, R. D.; Patterson, D. E.; Bunce, J. D. Comparative molecular field analysis (CoMFA). 1. Effect of shape on binding of steroids to carrier proteins. *J. Am. Chem. Soc.* **1988**, *110*, 5959–5967.

(33) Klebe, G.; Abraham, U.; Mietzner, T. Molecular similarity indices in a comparative analysis (CoMSIA) of drug molecules to correlate and predict their biological activity. *J. Med. Chem.* **1994**, *37*, 4130–4136.

(34) Klebe, G.; Abraham, U. Comparative molecular similarity analysis (CoMSIA) to study hydrogen-bonding properties and to score combinatorial libraries. *J. Comput.-Aided Mol. Des.* **1999**, *13*, 1–10.

(35) Rogers, D.; Hopfinger, A. J. Application of genetic function approximation to quantitative structure—activity relationships and quantitative structure—property relationships. *J. Chem. Inf. Comput. Sci.* **1994**, *34*, 854–866.

(36) Glen, W. G.; Dunn, W. J.; Scott, D. R. Principal components analysis and partial least squares. *Tetrahedron Comput. Meth.* **1989**, *2*, 349–376.

(37) *Catalyst*, version 4.6; Accelrys: Burlington, MA.

(38) Smellie, A; Teig, S. L.; Towbin, P. Poling: Promoting conformational coverage. *J. Comput. Chem.* **1995**, *16*, 171–187.

(39) Glide. http://www.schrodinger.com.